View metadata, citation and similar papers at core.ac.uk

brought to you by CORE

provided by Digital Repository @ Iowa State University

IOWA STATE UNIVERSITY
Digital Repository

Chemical and Biological Engineering Publications | Chemical and Biological Engineering

1994

Changes Produced by Cathodic Polarization in the Electrical Conduction Behavior of Surface Films on Aluminum

Ching-Feng Lin
Iowa State University

Kurt R. Hebert
Iowa State University, krhebert@iastate.edu

Follow this and additional works at: http://lib.dr.iastate.edu/cbe_pubs


Part of the Chemical Engineering Commons

The complete bibliographic information for this item can be found at http://lib.dr.iastate.edu/cbe_pubs/74. For information on how to cite this item, please visit http://lib.dr.iastate.edu/howtocite.html.

This Article is brought to you for free and open access by the Chemical and Biological Engineering at Digital Repository @ Iowa State University. It has been accepted for inclusion in Chemical and Biological Engineering Publications by an authorized administrator of Digital Repository @ Iowa State University. For more information, please contact digirep@iastate.edu.

51. P. Tarte, *Spectrochim. Acta,* **23A,** 2127 (1967).
52. J. Newman, *Electrochemical Systems,* p. 267, Prentice Hall, Inc., Englewood Cliffs, NJ (1991).
53. A. J. Bard and L. R. Faulkner, *Electrochemical Methods: Fundamentals and Applications,* p. 253, Wiley, New York (1980).
54. F. King and M. Spiro, *J. Solution Chem.,* **12,** 65 (1983).
55. M. Pourbaix, *Atlas of Electrochemical Equilibria in Aqueous Solutions,* p. 168, Pergamon Press, Ltd., Oxford (1966).

Changes Produced by Cathodic Polarization in the Electrical Conduction Behavior of Surface Films on Aluminum

Ching-Feng Lin[a] and Kurt R. Hebert*

Department of Chemical Engineering, Iowa State University, Ames, Iowa 50011

ABSTRACT

The electrochemical behavior of aluminum during cathodic polarization was investigated with the quartz crystal microbalance, to identify changes in the electrical conduction properties of the surface film, which result in strongly enhanced electrochemical reaction rates. As a consequence of cathodic charging at potentials more negative than about −1.45 V *vs.* NHE in 0.1*M* HCl solution, the surface film transforms from a high field electrical conductor to an ohmic conductor, and then begins to grow. The critical potential for forming this ohmically conducting film agrees with the potential below which aluminum hydroxide is expected to be more stable than aluminum oxide, near the metal/film interface. The conductivity of the cathodic film is within an order of magnitude of the proton conductivity of bulk hydrated aluminum hydroxide, $Al(OH)_3 \cdot H_2O$. When the potential is stepped above the open-circuit potential subsequent to cathodic charging, there is a characteristic current decay during several seconds, after which the conductivity is three orders of magnitude smaller than at the cathodic potential. A mechanism is given, based on calculated overpotentials for interfacial reaction and transport processes, through which the oxide film transforms to hydroxide at cathodic potentials.

There is a wide potential range on aluminum, of about 1.6 V, where both cathodic hydrogen evolution and anodic metal oxidation are thermodynamically possible. In acid solutions, near the open-circuit potential of about −0.8 V *vs.* the normal hydrogen electrode (NHE), the rates of anodic and cathodic reactions are limited by the resistance of the surface oxide film to transport of ions. However, at potentials more negative than about −1.2 V *vs.* NHE, there are greatly increased hydrogen evolution currents[1-7] and corrosion rates,[2,3,5,8] and surface films are deposited.[9] Also, in chloride ion containing solutions, the rate of corrosion pit initiation is observed to be greatly enhanced due to prior cathodic polarization of the metal below −1.2 V.[10] This effect may be responsible for the extremely large pit number densities found after alternating current (ac) etching of aluminum in chloride solutions.[10-13]

Two points of view have been adopted in explaining this cathodic activation of aluminum. Some investigators attribute the unusual cathodic behavior to increased pH in the solution near the metal surface, resulting from the cathodic decomposition of water to hydroxide ions.[2,6] The surface oxide film is known to be soluble in alkaline solutions, so the transport limitation imposed by the film on the rates of anodic and cathodic reactions would be removed. Films found to grow at cathodic potentials would have been precipitated on the electrode surface, due to the large metal dissolution rate. In contrast to this mechanism, others suggest that the surface oxide film becomes hydrated as a result of electrochemical processes occurring at cathodic potentials, and consequently its resistance dramatically decreases.[3,7,14]

In the preceding paper Lin *et al.*[15] used the electrochemical quartz crystal microbalance (QCM), together with infrared spectroscopy and capacitance measurements, to investigate the conditions for film growth at cathodic potentials. When the potential was held at −1.80 V (NHE) in 0.1*M* HCl solution, an oxyhydroxide or hydroxide surface film began to grow after the passage of only 7 mC/cm^2 of cathodic charge. Mass transport calculations showed that at the time film growth initiated, the solution near the electrode surface was practically unchanged from its initial composition. Thus, the film growth occurred by direct electrochemical reaction and not by precipitation from solution. Since the high resistance of the oxide film to ionic conduction would normally severely limit film growth at cathodic potentials, the original film must have undergone a structural transformation through which its electrical resistance had diminished greatly.

In the present work, the electrical conduction properties of the surface film on aluminum were measured before, during, and after cathodic polarization in 0.1*M* HCl solution. Measurements were carried out using the QCM, which allows the simultaneous monitoring of electrochemical charge and electrode mass changes, the latter with monolayer sensitivity.[16,17] Conductive properties of the surface film can be inferred, for example, through measurements of the variation of current flow with film mass during its growth. Also, a theoretical explanation is given for the transformation in the chemical composition of the film which led to the observed change in conduction behavior. The model for the film, on which this explanation is based, includes interfacial reactions and transport processes of aluminum and hydrogen ions, and the equilibrium between solid aluminum oxide and hydroxide in the film. Figure 1 is a schematic drawing of the film showing these reactions.

Experimental

Details of the QCM measurements and electrode preparation are the same as given in the preceding paper.[15] The aluminum electrodes were approximately 0.25 μm thick films evaporated from a pure source (99.99% Al foil, provided by KDK Corporation, Japan) onto AT-cut quartz crystals (Valpey-Fisher). The electrode area was 0.34 cm^2. The deposited films were exposed in laboratory ambient for 24 h. The crystals were then mounted into the wall of the electrochemical cell. A platinum wire and an Ag/AgCl/

* Electrochemical Society Active Member.
[a] Present address: Industrial Technology Research Institute, Materials Research Laboratories, Hsinchu, Taiwan, China.

Downloaded on 2014-02-10 to IP 129.186.176.91 address. Redistribution subject to ECS license or copyright; see ecsdl.org/site/terms_use

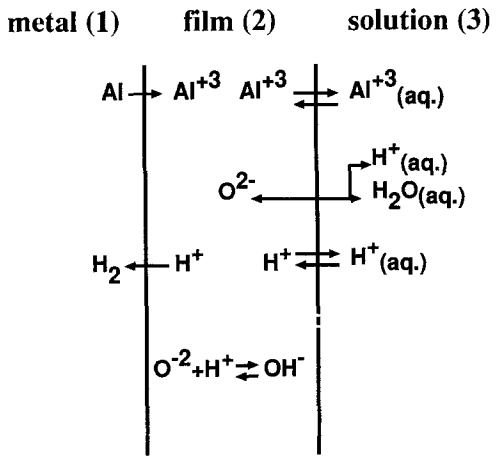

Fig. 1. Schematic representation of chemical and electrochemical reactions at the metal/film interface, in the film and at the film/solution interface.

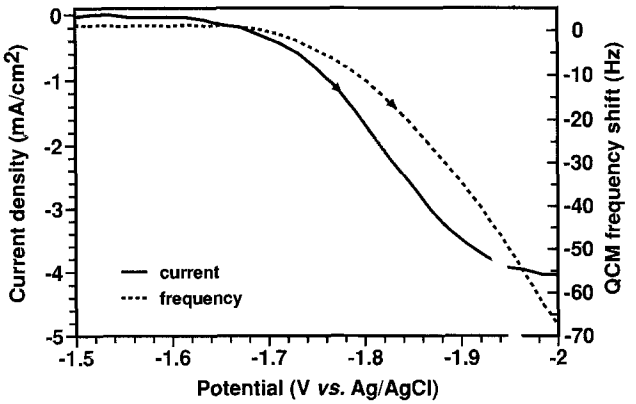

Fig. 2. Cathodic polarization curve and quartz crystal microbalance frequency shift, measured simultaneously during a potential sweep from −1.5 to −2.0 V. The solution was 0.1*N* HCl, and the potential scan rate was 10 mV/s.

4*M* KCl electrode were inserted into the cell as counterelectrode and reference electrode, respectively. Potentials given in this paper are relative to this reference electrode, unless otherwise stated. In all experiments the electrolyte was 25 ml aqueous 0.1*M* HCl solution at 25°C. Prior to polarization experiments, the aluminum electrode was allowed to contact with the electrolyte for 5 min at open circuit. This "pretreatment" was necessary to obtain significant currents and film growth during cathodic polarization. During QCM experiments, the interval between frequency measurements was 18 ms. Some other electrochemical current measurements were carried out without the QCM, using a potentiostat [Princeton Applied Research (PAR) 273]. Fast current transients were measured using a high speed voltmeter (Keithley 194A).

The crystals were operated at their fundamental resonant frequency of 5 MHz. Their mass sensitivity was 17.67 ngHz^{-1} cm^{-2}, according to Sauerbrey equation[16,17]

$$\Delta f = -2.26 \times 10^{-6} f^2 \Delta m \qquad [1]$$

where f is the resonant frequency of the quartz crystal in Hz, and Δm is the mass change in g/cm^2. This equation assumes that the surface film on the aluminum electrodes behaves as a rigid elastic overlayer and that there are no changes in the mechanical stress of the electrode during the experiments. These assumptions have been found to be valid in the present experiments.[15]

Results

Potentiodynamic cathodic polarization.—Electrochemical current and QCM frequency transients were measured simultaneously as the potential was swept between −1.5 and −2.0 V (Fig. 2). The potential scan was in the cathodic direction at a rate of 10 mV/s. No change in the QCM frequency was detected at potentials more positive than about −1.65 V, indicating that the electrode mass remained constant. However, as the potential became more cathodic than −1.65 V, the cathodic current rose and the frequency decreased with time (or potential). This decreasing frequency indicates an increase in electrode mass, according to Eq. 1.

Figure 3 shows a polarization curve plotted with a logarithmic current axis. The high current region was taken from the data in Fig. 2, while the low current region was measured separately, at higher sensitivity. Separate linear E *vs.* log i (Tafel) relationships exist in both potential regions. At potentials more cathodic than −1.8 V, the cathodic current falls below the high current Tafel line and approaches a plateau. This increase of kinetic resistance coincides with the significant buildup of mass in Fig. 2.

These kinetic data were corrected for the effect of ohmic potential drop by plotting log i against $(E_H - iR_\Omega)$, where E_H is the potential relative to a hydrogen electrode in equilibrium with the bulk solution. At the experimental pH of 1.25, E_H is 0.27 V more anodic than the potential measured experimentally. The cell resistance, R_Ω, had been determined to be 37 Ω-cm^2.[23] After this ohmic correction, the Tafel slope and exchange current density in the low current region (between −1.2 and −1.5 V) were −371 mV and 3.3 × 10^{-8} A/cm^2, respectively. In the high current region (between −1.65 and −1.79 V), the corrected Tafel slope and exchange current density were −96 mV and 5.7 × 10^{-19} A/cm^2.

Potentiostatic cathodic polarization.—Results of QCM measurements for potentiostatic cathodic charging were given previously.[15] In the present work these results are analyzed with the use of cathodic kinetic data from potentiodynamic polarization, to determine conduction properties of the surface film. Figure 4 shows the QCM frequency transient, as well as the charge passed, during cathodic charging at −2.0 V. After an initial period of about 2 s during which no frequency change was observed, the frequency decreased linearly with time, suggesting that cathodic products accumulated at a constant rate on the electrode surface. Lin *et al.*[15] presented infrared spectroscopy, surface capacitance, and oxide stripping measurements which confirmed that the frequency decrease was due to the deposition of a surface oxyhydroxide or hydroxide film. The cathodic current transient, corresponding to the QCM measurements in Fig. 4, is shown in Fig. 5. The current

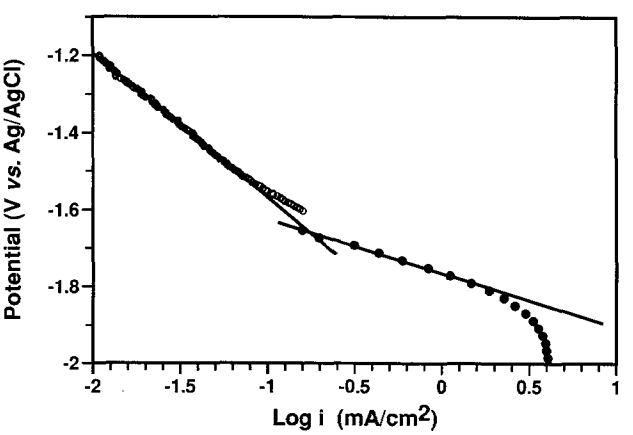

Fig. 3. Cathodic polarization curve for aluminum in 0.1*N* HCl, showing the two Tafel regions at low and high cathodic current. The data in the high current region (closed circles) are from Fig. 1; that in the low current region (open circles) were measured separately, at higher sensitivity. The potential scan rate in both regions was 10 mV/s. The Tafel lines are linear regression fits.

Downloaded on 2014-02-10 to IP 129.186.176.91 address. Redistribution subject to ECS license or copyright; see ecsdl.org/site/terms_use

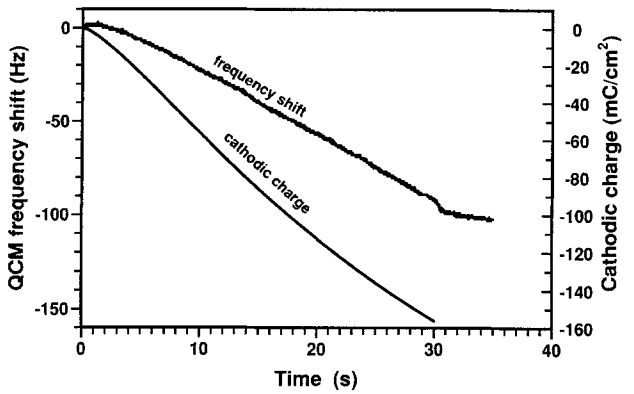

Fig. 4. Quartz crystal microbalance frequency transient and accumulated cathodic charge during cathodic polarization in 0.1 *N* HCl at −2.0 V. The potential was stepped directly to −2.0 V from the open-circuit potential and then to −0.9 V at 30 s.

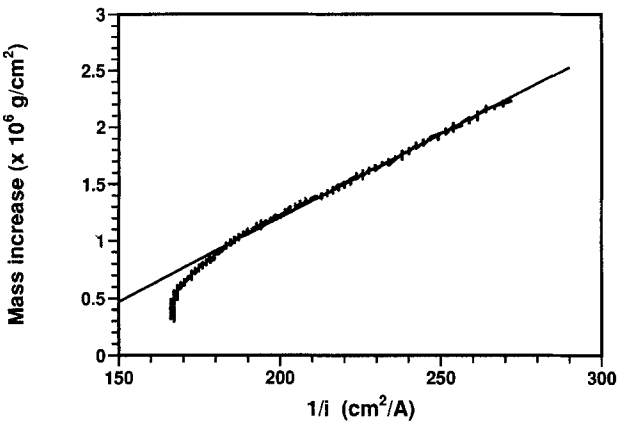

Fig. 6. Plot of transient mass increase during constant potential cathodic charging, *vs.* the reciprocal of the current density. The mass increase was calculated from the QCM frequency data in Fig. 4, during the period 7 to 30 s. The corresponding currents measured in the same experiment are from Fig. 5.

increased to a maximum of 6 mA/cm^2 at 7 s, and then began to decay.

As in the case of the potential sweep experiment, potentiostatic cathodic charging activated the aluminum surface. The initial cathodic current density in Fig. 5 is 1.7 mA/cm^2, which compares favorably to the current density of 1.1 mA/cm^2 calculated from the Tafel kinetic expression in the low current region in Fig. 3. The current density obtained from the other (high current) Tafel law, also at −2.0 V, is 5.5 mA/cm^2, which agrees with the maximum current of 6 mA/cm^2 in Fig. 5. Thus, the "activation" of the aluminum surface, that is, the transition between the two kinetic rate laws, took place over the initial period of 7 s in Fig. 5. The subsequent decrease in the cathodic current with time occurs during the buildup of the surface film indicated by the QCM results in Fig. 4.

According to Vijh,[18] during cathodic hydrogen evolution on aluminum, there is appreciable resistance to cathodic current flow in the surface film, and also to reduction at the metal/film interface. Both resistances influence the overall kinetic behavior. In agreement with this interpretation, the cathodic current was obtained by solving the current continuity equation

$$i_{Ho} \exp(-\beta_{12}\eta_H^{(12)}) = -\kappa \frac{\eta^{(2)}}{\delta} \qquad [2]$$

along with the equation relating the interfacial hydrogen overpotential to the cell potential E_H

$$E_H = \eta_H^{(12)} + \eta^{(2)} + iR_\Omega \qquad [3]$$

The superscript 12 in these equations refers to the metal/film interface, and 2 to the film itself (Fig. 1). The left side of Eq. 2 is the hydrogen reduction current at the metal/film interface, and the right side is the current through the film, which is driven by the overpotential in the film, $\eta^{(2)}$. Equation 2 incorporates the hypothesis that conduction in the film follows Ohm's law. In the preceding paper,[15] the film was found to have a duplex structure, with an inner layer with a large electrical resistance, and an outer, more conductive layer. κ in Eq. 2 is an average over these two layers, and is probably primarily determined by the resistive layer conductivity. Since the fraction of the total film thickness occupied by the resistive layer was approximately independent of film thickness, Eq. 2 treats κ as a material property of the surface film. Also, since the high cathodic current Tafel region in Fig. 3 occurs before significant film growth initiates, it is assumed that the current/potential relation in this region represents the kinetics of the hydrogen evolution reaction at the metal/film interface.

Equations 2 and 3 can be rearranged to yield a relationship between the cathodic mass increase and the current

$$\Delta m = \frac{\kappa\rho}{i}(E_H - \eta_H^{(12)}) - \rho(\kappa R_\Omega + \delta_o) \qquad [4]$$

Here, the film thickness δ was expressed as the sum of the initial film thickness δ_o and the thickness increase during cathodic charging $\Delta m/\rho$, where ρ is the film density and Δm is the film mass increase during cathodic charging. Equation 4 is hypothesized to govern the current decay during cathodic film growth. During this current decay, the expected variation of $\eta_H^{(12)}$, calculated from the kinetic parameters obtained from Fig. 3, is only 1.4%. Thus the term $(E_H - \eta_H^{(12)})$ in Eq. 4 is approximately a constant, and Δm is expected to be a linear function of $1/i$ if the film is an ohmic conductor. To test Eq. 4, film mass changes were calculated from the measured frequency shifts in Fig. 4, according to Eq. 1. After frequency shift was converted into mass units, it was multiplied by the "stripping ratio" of 1.38 to obtain the corresponding change in film mass. The stripping ratio represents the ratio of the frequency increase measured while chemically stripping the surface film, to the cathodic frequency decrease, and was found to be independent of cathodic charge.[15] This calculation may overestimate the film mass because of the possibility of an open-circuit film-forming reaction after cathodic charging.[15]

Figure 6 shows that the relationship between Δm and $1/i$ is in fact linear for times between 7 and 30 s in Fig. 4 and 5, which indicates that the film at these times is an ohmic conductor. The intercept of Fig. 6 is -1.47×10^{-6} g/cm^2. Using a film density of 2.4 g/cm^3 for aluminum hydroxide,[19] an initial film thickness 3.1 nm,[15] and a cell resistance of 37 Ω-cm^2,[23] a conductivity of 1×10^{-8} $(\Omega\text{-cm})^{-1}$ was calculated. This conductivity was then used to determine $\eta_H^{(12)}$

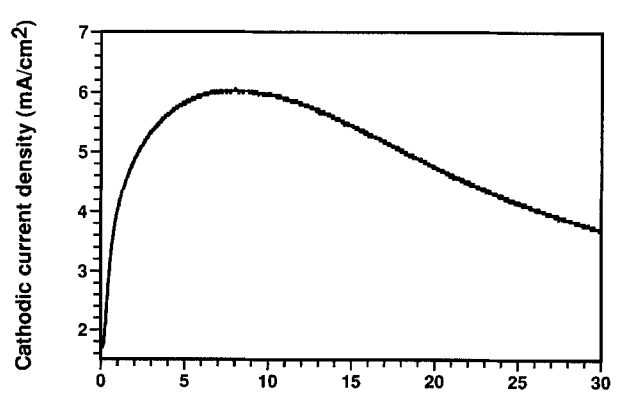

Fig. 5. Current transient during cathodic polarization in 0.1 *M* HCl at −2.0 V, for the same experiment shown in Fig. 4.

Downloaded on 2014-02-10 to IP 129.186.176.91 address. Redistribution subject to ECS license or copyright; see ecsdl.org/site/terms_use

from the slope of Fig. 6. An overpotential of −1.2 V was obtained, in reasonable agreement with the value of −1.5 V from the kinetic equation for the high current Tafel region. This agreement supports the assumption that this kinetic equation governs hydrogen reduction at the metal surface during film growth. As noted earlier, the conductivity given here is an effective value for the two-layer surface film. The thickness of the resistive layer, which controls the overall film resistance, was estimated as between 1/8 and 1/3 of the total film thickness; thus, the resistive layer conductivity might be as much as eight times smaller than the above value.

Anodic conduction before cathodic charging.—The next two sections discuss conduction measurements carried out at anodic potentials, before and immediately after cathodic polarization. Galvanostatic current step experiments were carried out to determine the anodic ion conduction rate law for the surface film prior to cathodic charging, following the method of Kirchheim.[20] These experiments were at potentials anodic enough to avoid complications from simultaneous cathodic hydrogen evolution. Since pitting corrosion would have occurred at these potentials in chloride solutions, the electrolyte solution was 0.05*M* H_2SO_4 instead of 0.1*M* HCl. Its pH of 1.35 was close to that of the HCl solution.

The initial anodic applied current was set to the "stationary corrosion current density," i_{co}, where the oxide growth/dissolution reaction

$$O^{-2}_{(f)} + 2H^{+}_{(aq)} \leftrightarrows H_2O_{(aq)} \qquad [5]$$

is at equilibrium. At i_{co}, the potential was constant with time, as expected. The current was stepped to a larger anodic current, i, held there for a time t_o, and then stepped back to i_{co}. As in the case of Kirchheim's measurements on iron,[20] after the current step to i, the potential immediately increased by ΔE_1, and thereafter increased linearly with time.

The analysis of these experiments followed Kirchheim's, and the reader is referred to his paper for a more detailed account. The initial potential increase ΔE_1 is supplied by increases in the potential drop across the film, and the overpotential at the film/solution interface

$$\Delta E_1 - \eta_o^{(23)} = \frac{\delta_o}{B_A} \ln \frac{i}{i_{co}} \qquad [6]$$

Equation 6 assumes that anodic conduction in the film obeys the high-field conduction law

$$i = i_{Ao} \exp\left(B_A \frac{\eta^{(2)}}{\delta}\right) \qquad [7]$$

where $\eta^{(2)}/\delta$ is the electric field in the film. A plot of $\Delta E_1 - \eta_o^{(23)}$ *vs.* ln (i/i_{co}) from the present experimental data is shown in Fig. 7. $\eta_o^{(23)}$ and i_{co} were calculated using kinetic

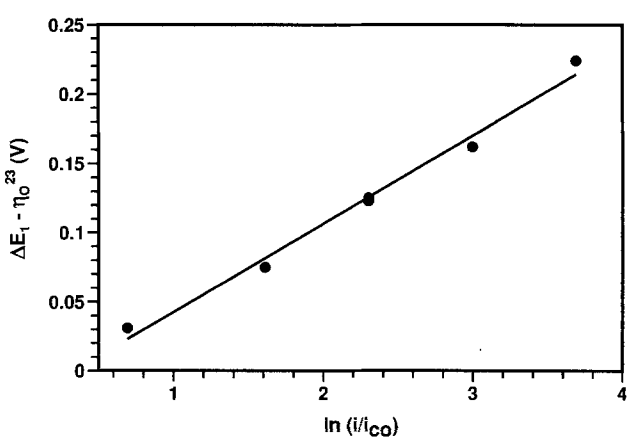

Fig. 7. Plot representing variation of anodic current with ion transport overpotential in the film, prior to cathodic polarization. The ordinate and abscissa are according to Eq. 6 in the text. The experiments were carried out in 0.05*M* H_2SO_4 solution.

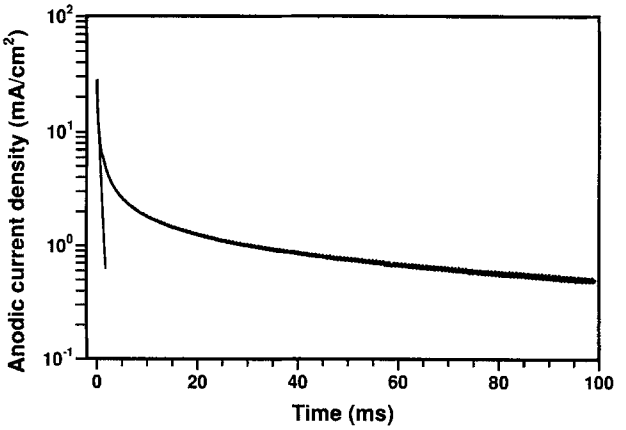

Fig. 8. An early period of an anodic current transient following a potential step to −0.9 V, after cathodic polarization at −2.0 V. Cathodic charging was for a period of 3 s (11.2 mC/cm² cathodic charge passed). The experiment was in 0.1*N* HCl.

expressions for the oxide growth/dissolution reaction, and the dissolution of aluminum ions from the film. These expressions were written in the forms given previously for the corresponding reactions on iron;[20,21] kinetic parameters for aluminum were taken from the measurements of Våland and Heusler,[22] as discussed in greater detail by Lin.[23] The linearity of Fig. 7 shows that the high-field conduction equation was in fact obeyed for anodic conduction before cathodic charging. The high field constant B_A, calculated from the slope of Fig. 7 along with the value of the initial film thickness, δ_o = 3.1 nm, was 4.9×10^{-6} cm/V. In good agreement with this value, Videm[24] reported B_A to be 4.7×10^{-6} cm/V for both native oxide films and anodic films, and Young[25] gave a value of 3.8×10^{-6} cm/V for anodic films.

Anodic conduction characteristics of the film formed by cathodic charging.—The anodic conduction behavior of the film produced by cathodic polarization was determined from the current transients measured upon stepping to an anodic potential after cathodic charging. An example of the early time portion of such a current transient is shown in Fig. 8, where the current is plotted on a logarithmic axis. Lin *et al.*[15] showed that the exponential current decay approached asymptotically at early times (indicated by the straight line in Fig. 8) was due to capacitive charging of the part of the film near the metal surface.

Since cathodic conduction in this film was ohmic, the initial anodic conduction also may follow Ohm's law. The relation between the current and the measured potential E_H would then be

$$\eta^{(2)} = \frac{i\delta}{\kappa} = E_H - \eta_o^{(23)} - iR_\Omega - E^* \qquad [8]$$

E^* is a constant term which includes equilibrium potentials for aluminum metal oxidation and dissolution from the film. It is assumed that the overpotential for metal ionization ($\eta_{Al}^{(12)}$) is small compared to the other terms and can be neglected. The hypothesis of ohmic conduction was tested by plotting $i\delta$, the product of the initial current and the film thickness, against the corrected potential $E_H - \eta_o^{(23)} - iR_\Omega$. This "initial current" was taken to be the first current measured with the QCM data acquisition system, at a time of 4 ms; this time is well beyond the capacitive relaxation depicted in Fig. 8. $\eta_o^{(23)}$ was calculated from the measured anodic current, as in the previous section. The film thickness δ at the beginning of the anodic period was determined as in Fig. 6.

Figure 9 shows the plot of $i\delta$ *vs.* the corrected anodic potential. The potential range in the figure corresponds to experimentally measured potentials between −0.9 and −0.2 V *vs.* the Ag/AgCl reference electrode. The linearity of the current over this wide potential range, as expected from Eq. 8, is evidence that conduction in the film is ohmic. The variation in film thickness between the experiments was about 17%. The film conductivity calculated from the slope

Downloaded on 2014-02-10 to IP 129.186.176.91 address. Redistribution subject to ECS license or copyright; see ecsdl.org/site/terms_use

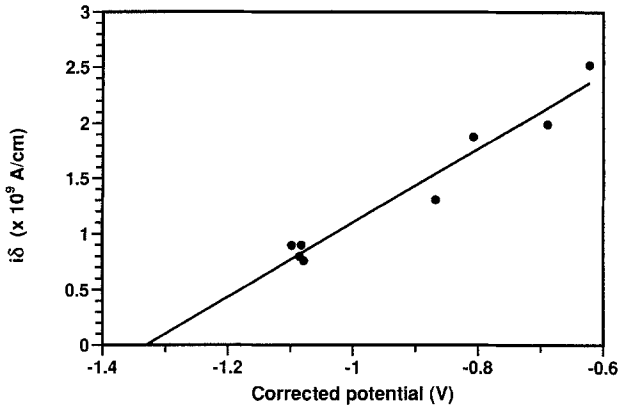

Fig. 9. Dependence of $i\delta$, the product of the initial anodic faradaic current density and the film thickness, on potential. Cathodic polarization was for a period of 10 s at −2.0 V, after which the potential was stepped to various anodic values. The currents in the figure were measured at a time of 4 ms after the anodic step, which is much longer than the time for capacitive charging of the electrode surface. The solution in all cases was 0.1*M* H_2SO_4. Anodic potentials were corrected by subtracting $\eta_O^{(23)}$ and the ohmic potential drop iR_Ω, according to Eq. 8.

in Fig. 9 is 3×10^{-9} $(\Omega\text{-cm})^{-1}$, three times smaller than the conductivity of 1×10^{-8} $(\Omega\text{-cm})^{-1}$ from Fig. 6, for cathodic conduction in the same film. The result that both anodic and cathodic conductivities are on the same order of magnitude confirms that the film formed during cathodic charging is in general an ohmic ionic conductor. The apparently smaller anodic conductivity is partly the result of the current decay between 1 ms, just after the capacitive relaxation, and 4 ms, when the current was measured. Accounting for this decay, the "initial conductivity" should be about twice the reported value, or 6×10^{-9} $(\Omega\text{-cm})^{-1}$.

The steady-state currents after the anodic current transients were on the order of 10 $\mu A/cm^2$. Figure 10 shows these final currents plotted in the same way as in Fig. 9. The current again depends linearly on potential over a wide range, indicating ohmic conduction behavior. However, the conductivity from the slope of Fig. 9 is 4×10^{-12} $(\Omega\text{-cm})^{-1}$, about three orders of magnitude lower than the conductivity immediately after cathodic charging. In addition to this markedly decreased conductivity, the open-circuit potential after the anodic transient increased by about 0.5 V.

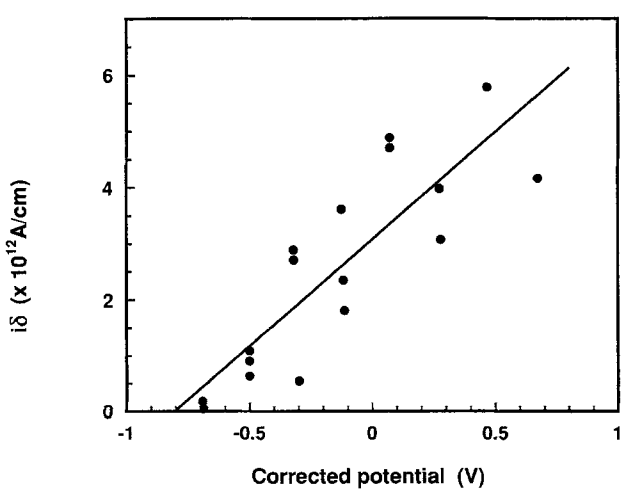

Fig. 10. Dependence of the steady-state anodic current density on anodic potential. The conditions of these experiments were the same as for Fig. 9, and the potentials were corrected in the same way. Corrections for film thickness variations between experiments were not made; the film thickness was calculated from the QCM data in Fig. 4, and was assumed to be the same in every experiment. The steady-state currents were reached at times of typically 30 s after the anodic potential step.

Discussion

Electrical conduction behavior of the film.—The cathodic polarization curve (Fig. 2) shows that the Tafel slope for hydrogen evolution decreases significantly at potentials more negative than about −1.7 V. A calculation is given here which shows that this change of the Tafel slope is consistent with a reduction in the resistance for current flow in the film, while the kinetic resistance at the metal/film interface is unchanged.

For the low current Tafel region (anodic to −1.7 V), it is proposed that cathodic conduction, like anodic conduction in the same film, follows the high field conduction equation

$$i = -i_{Co} \exp\left(\frac{-B_C \eta^{(2)}}{\delta}\right) \qquad [9]$$

where B_C is the cathodic high-field conduction coefficient. When the current density in Eq. 9 is set equal to the reaction current density at the metal/film interface (Eq. 2), an exponential (Tafel) rate law is obtained for the cathodic current in terms of the combined overpotential, $\eta_H^{(12)} + \eta^{(2)}$

$$i = -i_{Co}\left(\frac{i_{Co}}{i_{Ho}}\right)^{\frac{-B_C}{\delta\beta_{12}+B_C}} \exp\left[\frac{-\beta_{12}B_C}{\delta\beta_{12}+B_C}(\eta_H^{(12)} + \eta^{(2)})\right] \qquad [10]$$

It is assumed that the kinetic parameters of the electrochemical reaction (β_{12} and i_{Ho}) are the same in both Tafel regions; their values were therefore determined from the high current Tafel region, in which the film resistance is small. The conduction parameters in Eq. 10 were then obtained from the Tafel equation for the low current region. B_C and i_{Co} were found to be 2.6×10^{-6} cm/V and 0.17 mA/cm^2, respectively.

This calculated B_C is a factor of 1.9 smaller than B_A, the high-field coefficient for anodic conduction in the same film. According to the theory of high-field conduction,[20] the ratio B_A/B_C should be z_A/z_C, the ratio of charge numbers of the current-carrying species during anodic and cathodic conduction. (This prediction assumes that the potential energy barriers for cathodic and anodic conduction are the same.) The cathodic current carrier is likely to be the proton; during anodic oxidation, 50 to 80% of the current is carried by oxide ions, and the rest by metal ions.[26] Therefore, B_A/B_C should probably be in the range 2.2 to 2.5, in good agreement with the experimental value of 1.9. Since the cathodic and anodic conduction equations are mutually consistent, the large Tafel slope at potentials above −1.7 V can be attributed to the high cathodic conduction resistance of the film.

Conduction in the film during polarization at lower potentials was found to follow Ohm's law. Infrared spectroscopy and QCM film stripping experiments had previously found that the film after cathodic charging was an oxyhydroxide or hydroxide which contained appreciable amounts of water.[15] Dzimitrowicz *et al.*[27] showed that bulk $Al(OH)_3 \cdot H_2O$ is an ohmic proton conductor, with a conductivity of 6×10^{-8} $(\Omega\text{-cm})^{-1}$, on the same order of magnitude as the conductivity during cathodic charging, 1×10^{-8} $(\Omega\text{-cm})^{-1}$. The comparison of these conductivities is justifiable, since protons probably carry current through the cathodic film. The aluminum hydroxide studied by Dzimitrowicz *et al.* was obtained by neutralization of $Al(NO_3)_3$ solution; this material has low crystalline order and very small hydroxide particle sizes.[28] Additional water molecules occupy its interparticle spaces to produce a connected, viscous-liquid region through the material, through which the current was considered to flow. The similar conductivity of the cathodic film therefore suggests that it may also have connected aqueous pathways, which are responsible for its ohmic conduction behavior.

After stepping to an anodic potential, ohmic conduction in the film was maintained, but the conductivity decreased by three orders of magnitude. If the large cathodic conductivity is attributed to its high water content, then the loss of conductivity may be due to the removal of this entrained water, possibly as the result of reaction between it and the metal, to form solid aluminum oxide or hydroxide.

Downloaded on 2014-02-10 to IP 129.186.176.91 address. Redistribution subject to ECS license or copyright; see ecsdl.org/site/terms_use

Mechanism of chemical transformation of the film.—The onset of film growth and increased currents at cathodic potentials is explained in this section. The rates of electrochemical metal oxidation and hydrogen evolution at the metal/film interface are governed by the overpotentials $\eta_{Al}^{(12)}$ and $\eta_{H}^{(12)}$, respectively. These overpotentials are defined according to the electrochemical potentials of ions in the film near the interface

$$3F\eta_{Al}^{(12)} = \mu_{Al} - 3\mu_{e^-} - \mu_{Al^{+3}}^{(12)} \quad [11]$$

$$F\eta_{H}^{(12)} = \frac{1}{2}\mu_{H_2} - \mu_{e^-} - \mu_{H^+}^{(12)} \quad [12]$$

The aluminum and hydrogen overpotentials are not independent. The relation between them can be expressed in terms of the film composition near the metal/film interface

$$\eta_{H}^{(12)} = \eta_{Al}^{(12)} + \frac{1}{3F}(\mu_{Al_2O_3}^{(21)} - \mu_{Al(OH)_3}^{(21)}) \quad [13]$$

This equation assumes that hydroxide, hydrogen, and oxide ions are in equilibrium in the film

$$\mu_{OH^-} = \mu_{H^+} + \mu_{O^{-2}} \quad [14]$$

Further, the electrochemical potentials of Al^{+3}, O^{-2}, and OH^- ions have been related to the chemical potentials of the neutral compounds, Al_2O_3 and $Al(OH)_3$, by dissociation equilibria. As a first approximation, the film is taken to be an ideal mixture of its components, aluminum oxide and hydroxide, and water. In this case, μ_i, the chemical potential of component i in the film, is $\mu_i^\circ + RT \ln x_i$, where x_i is the mole fraction of the species. Equation 13 then becomes

$$\eta_{H}^{(12)} = \eta_{Al}^{(12)} + \frac{1}{3F}(\mu_{Al_2O_3}^{\circ} - \mu_{Al(OH)_3}^{\circ}) + \frac{RT}{3F}\ln\left(\frac{x_{Al_2O_3}}{x_{Al(OH)_3}}\right)$$

$$= \eta_{Al}^{(12)} - 1.57\ \text{V} + (8.56\ \text{mV})\ln\left(\frac{x_{Al_2O_3}}{x_{Al(OH)_3}}\right) \quad [15]$$

The standard chemical potentials of Al_2O_3 and $Al(OH)_3$ were taken as −380.5 and −271.9 kcal/mol, respectively.[29] Previous models for oxide films on metals have assumed that the overpotential for metal atom ionization ($\eta_{Al}^{(12)}$) is zero;[20] the same assumption is made here (except during the initial moments of cathodic charging, as discussed below). Thus, the ratio of mole fractions in Eq. 15 varies from 100 at $\eta_{H}^{(12)}$ = 1.53 V to 0.01 at −1.61 V. The thermodynamic transition from Al_2O_3 to $Al(OH)_3$ thus occupies a narrow potential range around $\eta_{H}^{(12)} = -1.57$ V. This critical $\eta_{H}^{(12)}$ can be compared to the potential of about −1.75 V *vs.* Ag/AgCl in Fig. 2 at which the hydrogen evolution is "activated" and film growth begins. Neglecting $\eta^{(2)}$ in the low resistance film which is present after the transition, the value of $\eta_{H}^{(12)}$ at −1.75 V is −1.48 V, in very good agreement with Eq. 15. Thus the markedly decreased ion transport resistance in the film below −1.75 V coincides with the thermodynamic expectation of a hydroxide, rather than oxide film at these potentials.

The mechanism of the transformation of the film composition from an oxide into a hydroxide can be understood using Eq. 15. Immediately after the step from the open-circuit potential ($E_H \approx -0.53$ V) to the cathodic potential (E_H = −1.73 V, corresponding to −2.0 V *vs.* Ag/AgCl), the film composition term in Eq. 15 had not begun to change; therefore, the changes in $\eta_{Al}^{(12)}$ and $\eta_{H}^{(12)}$ were equal. In order to supply the initial cathodic current of 1.1 mA/cm^2, the initial $\eta_{H}^{(12)}$ at the cathodic potential was −1.5 V, according to the reaction kinetic expression from Fig. 3. Thus, the changes of both $\eta_{H}^{(12)}$ and $\eta_{Al}^{(12)}$ at the potential step were at least −1.0 V; as a result, $\eta_{Al}^{(12)}$ was about −1.0 V at the beginning of the cathodic period. Since the cathodic applied potential was close to the equilibrium potential of aluminum (E_H = −1.65 V), the negative $\eta_{Al}^{(12)}$ was compensated by an overpotential of about 1.0 V through the film. The cathodic $\eta_{Al}^{(12)}$ prevented aluminum oxidation at the metal/film interface, while the large positive film overpotential continued to drive Al^{+3} transport out through the film; consequently, the aluminum ion concentration near the metal/film interface decreased with time. To preserve electrical neutrality, the depletion of aluminum ions was compensated by the inward movement of protons, which were transferred to oxide ions near the metal/film interface (Eq. 14), forming hydroxide ions. As the film composition near the metal surface shifted from hydrated aluminum oxide toward aluminum hydroxide, the composition term in Eq. 15 became more negative, causing $\eta_{Al}^{(12)}$ to become less cathodic ($\eta_{H}^{(12)}$ is approximately constant, as discussed above), and eventually reach zero. At this point, aluminum oxidation began, and film growth initiated. The highly conductive nature of the cathodic film is probably attributable to pores created by dissolution of the hydroxide film material from the film/solution interface, as film growth proceeds from the metal/film interface.

Conclusions

When aluminum is polarized to potentials more cathodic than about −1.5 V *vs.* NHE, cathodic currents are significantly enhanced, and the surface film begins to grow. The work reported here explored the relation between this cathodic "activation" and the electrical resistance of the surface film. Cathodic polarization at −2.0 V *vs.* Ag/AgCl was found to transform the film from a high field (exponential) to an ohmic ion conductor. The conductivities for both cathodic and anodic current flow were on the order of 10^{-8} $(\Omega\text{-cm})^{-1}$, and agree with the conductivity of bulk hydrated aluminum hydroxide, as measured by Dzimitrowicz *et al.*[27] The conduction mechanism is believed to be similar to that of the bulk hydroxide in that current flows primarily through connected aqueous pathways. Indeed, in the preceding investigation using infrared spectroscopy and QCM stripping measurements, the hydration of the cathodic film was found to be significant. When the potential is returned to values near the open-circuit potential, the conductivity increases by a factor of 10^3 in a time of several seconds.

An equation was derived which relates the overpotentials of the electrochemical reactions at the metal/film interface (cathodic hydrogen evolution and anodic metal oxidation), and the film composition there. The critical potential for cathodic activation was shown to coincide with the potential below which aluminum hydroxide is thermodynamically stable relative to aluminum oxide, at the metal/film interface. Conversion of oxide to hydroxide proceeds from the inner portion of the film, as ionic transport processes cause aluminum ions to be replaced by protons. The high conductivity of the hydroxide film can be explained by partial dissolution from the film/solution interface into the acidic electrolyte solution, which leads to a porous film structure.

Acknowledgments

Financial support for this work was provided by KDK Corporation (Takahagi, Japan) through a fellowship to Mr. Lin. M.-H. Wang carried out the experiments whose results are shown in Fig. 10. The authors thank M. D. Porter for allowing the use of the vacuum evaporation system for fabrication of aluminum electrodes.

Manuscript submitted April 29, 1993; revised manuscript received Sept. 17, 1993.

Iowa State University assisted in meeting the publication costs of this article.

LIST OF SYMBOLS

B_A, B_C	anodic and cathodic high field conduction coefficients, cm/V
E_H	potential of the aluminum electrode relative to a hydrogen electrode in equilibrium with the bulk solution, V
E^*	constant potential, V
F	Faraday constant, 96,487 C/equivalent
f	resonant frequency of quartz crystal microbalance, Hz
i	current density, A/cm^2

Downloaded on 2014-02-10 to IP 129.186.176.91 address. Redistribution subject to ECS license or copyright; see ecsdl.org/site/terms_use

i_{Ao}, i_{Co}	pre-exponential current densities for anodic and cathodic high field conduction, A/cm^2
i_{co}	exchange current density for metal ion transfer reaction at the film/solution interface, A/cm^2
i_{Ho}	exchange current density for hydrogen evolution at the metal/film interface, A/cm^2
R	gas constant 8.314 J/mol-K
R_Ω	cell ohmic resistance, Ω-cm^2
T	absolute temperature, K
x_i	mole fraction of species i, dimensionless
Greek	
β_{12}	kinetic parameter for hydrogen evolution at the metal/film interface, V^{-1}
ΔE_1	initial potential increase in anodic current step experiments, V
Δm	mass change, g/cm^2
δ	surface film thickness, cm
δ_0	initial surface film thickness, cm
$\eta_i^{(jk)}$	overpotential of reaction i at interface between phases j and k, V
$\eta^{(2)}$	overpotential driving current through the surface film, V
κ	conductivity, (Ω-cm)$^{-1}$
$\mu_i^{(jk)}$	chemical or electrochemical potential of species i, near interface between phases j and k (on j side of the interface), J/mol
μ_i°	standard chemical potential of species i, J/mol
ρ	density of surface film, g/cm^3

REFERENCES

1. M. J. Pryor and D. S. Keir, *This Journal,* **102,** 605 (1955).
2. H. Kaesche, *Werkst. Korros.,* **14,** 557 (1963).
3. J. Kunze, *Corros. Sci.,* **7,** 273 (1967).
4. J. W. Diggle, T. C. Downie, and C. W. Goulding, *ibid.,* **8,** 907 (1968).
5. G. A. DiBari and H. J. Read, *Corrosion,* **27,** 483 (1971).
6. R. Grauer and E. Wiedmer, *Werkst. Korros.,* **24,** 128 (1973).
7. K. Nisancioglu and H. Holtan, *Electrochim. Acta,* **24,** 1229 (1979).
8. E. P. G. T. van de Ven and H. Koelmans, *This Journal,* **123,** 143 (1976).
9. W. Vedder and D. A. Vermilyea, *Trans. Faraday Soc.,* **65,** 561 (1969).
10. C.-F. Lin and K. R. Hebert, *This Journal,* **137,** 3723 (1990).
11. G. E. Thompson and G. C. Wood, *Corros. Sci.,* **18,** 721 (1978).
12. C. K. Dyer and R. S. Alwitt, *This Journal,* **128,** 300 (1981).
13. H. Terryn, J. Vereecken, and G. E. Thompson, *Corros. Sci.,* **32,** 1159 (1991).
14. J. Radošević, M. Kliškić, P. Dabić, R. Stevanović, and A. Despić, *J. Electroanal. Chem.,* **277,** 105 (1990).
15. C.-F. Lin, M. D. Porter, and K. R. Hebert, *This Journal,* **141,** 96 (1994).
16. D. A. Buttry, in *Electroanalytical Chemistry: A Series of Advances,* A. J. Bard, Editor, p. 1, Marcel Dekker, Inc., New York (1991).
17. D. A. Buttry and M. D. Ward, *Chem. Rev.,* **92,** 1355 (1992).
18. A. K. Vijh, *J. Phys. Chem.,* **73,** 506 (1969).
19. *CRC Handbook of Chemistry and Physics,* 71st ed., D. R. Lide, Editor, pp. 4-41, CRC Press, Boston, MA (1990).
20. R. Kirchheim, *Electrochim. Acta,* **32,** 1619 (1987).
21. K. J. Vetter and F. Gorn, *ibid.,* **18,** 321 (1973).
22. T. Våland and K. E. Heusler, *J. Electroanal. Chem.,* **149,** 71 (1983).
23. C.-F. Lin, Ph.D. Thesis, Iowa State University, Ames, IA (1992).
24. K. Videm, *The Electrochemistry of Uniform Corrosion and Pitting of Aluminum,* Kjeller Report, p. 37, Institutt for Atomenergi, Kjeller, Norway (1974).
25. L. Young, *Anodic Oxide Films,* p. 220, Academic Press, Inc., New York (1961).
26. M. J. Dignam, in *Oxides and Oxide Films,* Vol. 1, J. Diggle, Editor, p. 203, Marcel Dekker, Inc., New York (1973).
27. D. J. Dzimitrowicz, J. B. Goodenough, and P. J. Wiseman, *Mater. Res. Bull.,* **17,** 971 (1982).
28. K. Wefers and C. Misra, *Oxides and Hydroxides of Aluminum,* Alcoa Technical Paper No. 19, Revised, p. 3, Alcoa Laboratories (1987).
29. M. Pourbaix, *Atlas of Electrochemical Equilibria in Aqueous Solutions,* p. 168, Pergamon Press, Oxford (1966).

Downloaded on 2014-02-10 to IP 129.186.176.91 address. Redistribution subject to ECS license or copyright; see ecsdl.org/site/terms_use